Human Activities Caused Hypoxia Expansion in a Large Eutrophic 1 **Estuary: Non-negligible Role of Riverine Suspended Sediments** 2 3 Yue Nan¹, Zheng Chen², Bin Wang³, Bo Liang⁴, Jiatang Hu^{1,5,6*} 4 5 ¹ School of Environmental Science and Engineering, Sun Yat-Sen University, 6 7 Guangzhou, 510275, China ² Earth, Ocean and Atmospheric Sciences Thrust, The Hong Kong University of 8 9 Science and Technology (Guangzhou), Guangzhou, 511455, China ³ Department of Oceanography, Dalhousie University, Halifax, Nova Scotia, Canada 10 ⁴ Eco-Environmental Monitoring and Research Center, Pearl River Valley and South 11 12 China Sea Ecology and Environment Administration, Ministry of Ecology and Environment of the People's Republic of China, Guangzhou, 510611, China 13 ⁵ Guangdong Provincial Key Laboratory of Environmental Pollution Control and 14 Remediation Technology, Guangzhou, 510275, China 15 ⁶ Southern Marine Science and Engineering Guangdong Laboratory (Zhuhai), Zhuhai, 16 17 519000, China

Correspondence: Jiatang Hu (hujtang@mail.sysu.edu.cn)

18

19 20

21 Abstract

22

23

24

25

26

27

28

29

30

31

32

33

34

35

36

37

38

39

40

41

42

43

44

45

46

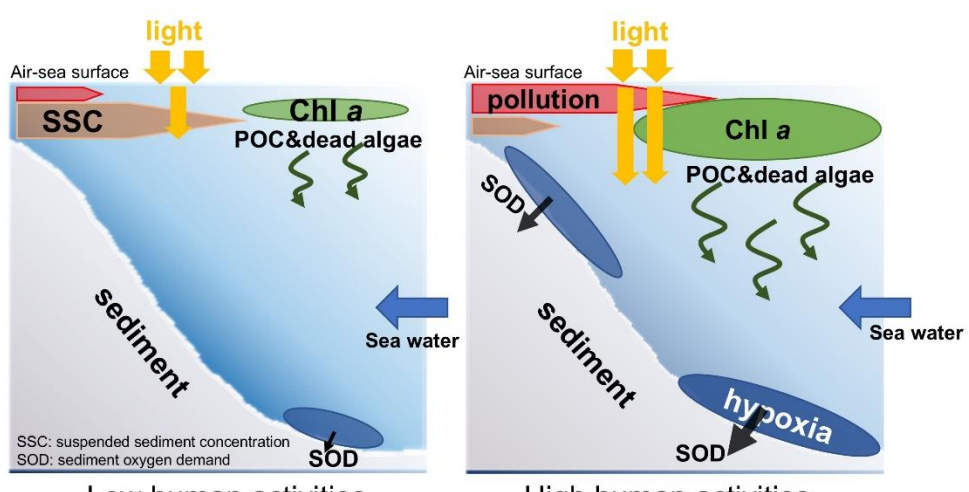
47

48

Increase in riverine nutrient loads was generally recognized as the primary cause of coastal deoxygenation, whereas the role of other riverine factors, especially suspended sediments, has received less attention. This study aims to discern the impacts of anthropogenic alterations in various riverine inputs on the subsurface deoxygenation over the past three decades in a large river-dominated estuary, the Pearl River Estuary (PRE). By utilizing the physical-biogeochemical model, we reproduced the observed dissolved oxygen (DO) conditions off the PRE in the historical period (the 1990s with high-suspended sediments-DO and low-nutrient inputs) and the present period (the 2010s with low-suspended sediments-DO and high-nutrient inputs). Due to the decadal changes in riverine inputs, the PRE has witnessed more extensive and persistent lowoxygen events during summer in the 2020s, with larger spatial extents of ~2926 km² for low oxygen (DO \leq 4 mg/L, increased by \sim 148% relative to the 1990s) and 617 km² for hypoxia (DO \leq 3 mg/L, by 192%) and longer duration (by \sim 15-35 days), evolving into three distinct hypoxic centers controlled by different factors. Model experiments suggested that the decreased riverine DO content (46%) has led to a low-oxygen expansion in the upper regions, accounting for 44% to the total increment. Meanwhile, the increased nutrient levels (100% in nitrogen and 225% in phosphorus) and the declined suspended sediment concentration (60%) have jointly promoted the primary production and bottom oxygen consumptions (dominated by sediment oxygen uptake), thus resulting in a substantial enlargement of low-oxygen area (104%) and hypoxic area (192%) in the lower reaches. Our results revealed a more critical role of the riverine suspended sediment decline in the exacerbation of eutrophication and deoxygenation off the PRE via improving light conditions to support higher local productivity, which could further amplify the effect combined with the growth in nutrients and confound the effectiveness of hypoxia mitigation under nutrient controls. Overall, in the context of global changes in riverine suspended sediments, it is imperative to reassess the contribution of riverine inputs to the coastal deoxygenation worldwide over the past

- decades, given that the impact of suspended sediments has been constantly overlooked
- in relevant investigations.
- 51 Key words: Deoxygenation; suspended sediments; nutrient inputs; decadal changes;
- 52 Pearl River Estuary

53 Graphical Abstract



Low human activities

High human activities

55 1. Introduction

54

56

57

58

59

60

61

62

63

64

65

66

Hypoxia emerges when dissolved oxygen (DO) concentration drops below 3 mg/L in aquatic systems. It is an undesirable phenomenon which can lead to a series of biological and ecological consequences, such as damaging the habitat for aquatic organisms and imposing detrimental effects on the ecosystem community structure (Diaz and Rosenberg, 2008; Roman et al., 2019). Due to the substantial impacts from human socioeconomic activities, coastal regions have become a hotspot for hypoxia (Breitburg et al., 2018; Pitcher et al., 2021). Moreover, long-term exacerbation of hypoxia with spatial expansion and increased intensity has been frequently reported in estuarine and coastal regions worldwide during the past decades, including the Baltic Sea (Carstensen et al., 2014), the northern Gulf of Mexico (Bianchi et al., 2010), Chesapeake Bay (Murphy et al., 2011), the Yangtze River Estuary (Chen et al., 2017),

and the Pearl River Estuary (Hu et al., 2021).

67

68

69

70

71

72

73

74

75

76

77

78

79

80

81

82

83

84

85

86

87

88

89

90

91

92

93

94

Plenty of studies were conducted to reveal the mechanism of hypoxia formation and evolution in coastal regions. It has been widely recognized that coastal deoxygenation is largely attributed to the eutrophication-driven production of organic matters (Su et al., 2017; Wang et al., 2016; Howarth et al., 2011), which sink to the subsurface waters and bottom sediments, leading to intense oxygen depletion (Wang et al., 2014; Hagy et al., 2005). This would induce hypoxia when the density stratification restricts DO replenishment from the surface waters (Wang et al., 2018; Murphy et al., 2011). One important reason underlying eutrophication and hypoxia is the excessive nutrients that are discharged into the water column and stimulate phytoplankton blooms (Cullen, 2015; Wang et al., 2021; Cormier et al., 2023). Human activities, such as dam construction (Bussi et al., 2021) and soil-water conservation measures (Yang et al., 2024) can significantly reduce suspended sediment in estuaries. In addition, an improved light condition, e.g., due to the decreased suspended sediment loads, could also favor the enhancement of local production and hence hypoxia (Ge et al., 2020; Huang et al., 2022). The effects of nutrient and light conditions vary in coastal systems due to different hydrodynamic and topographic features, which makes the formulation of hypoxia mitigation strategies more challenging. Therefore, a quantitative assessment on the importance of these factors in generating hypoxia is crucial for understanding the primary drivers of hypoxia evolution and for proposing effective countermeasures. A case in point is the Pearl River Estuary (PRE), which is situated in the northern South China Sea and close to the Guangdong-Hong Kong-Macao Great Bay Area (Fig. 1a). Owing to the relatively large nutrient inputs and vertical stratification formed by freshwater plume, hypoxia typically occurs during summer in the bottom waters of the PRE. Before the 2000s, it was an episodic and small-scale issue because of the synergetic effect of shallow topography, high turbidity (Ma et al., 2022), and the intermittent stratification due to periodic disturbance by the tides. However, large-scale occurrences of low oxygen (when DO < 4 mg/L) and hypoxia were frequently reported

in recent years. For example, it was estimated that the low-oxygen area within the PRE achieved 1000 km² and 1500 km² during summer in 2010 (Wen et al., 2020) and 2015 (Li et al., 2018), respectively, which were nearly double to that before the 2000s (Li et al., 2020). Hu et al. (2021) compiled historical observations over four decades to investigate the long-term deoxygenation trend and its spatial expansion in the PRE. They highlighted the significant contributions of increased nutrient and decreased sediment fluxes from the Pearl River to the exacerbation of low-oxygen conditions in the region. Besides, the low-oxygen inflows from the Pearl River could also contribute to the low-oxygen area in the upper estuary (Hu et al., 2021). Nevertheless, a quantitative understanding of their relative contributions to the low-oxygen expansion in the PRE is lacking, particularly in different subregions (Fig.1b) where the mechanisms controlling the low-oxygen conditions are different. In the upper part of the PRE (Lingdingyang waters), aerobic respiration of terrestrial organic matter plays a greater role (Su et al., 2017; Yu et al., 2020); in the downstream regions of the PRE, deoxygenation is primarily controlled by eutrophication (Yu and Gan, 2022; Chen et al., 2024). In this study, we used a coupled physical-biogeochemical model to investigate the

In this study, we used a coupled physical-biogeochemical model to investigate the decadal changes (the 1990s versus the 2010s) in summertime DO contents and related biogeochemical processes in the PRE and to quantify the relative contributions of the changing riverine inputs (including nutrients, suspended sediments, and oxygen content; Fig. 1c-f) to the long-term expansion of low oxygen (DO < 4 mg/L) and hypoxia (DO < 3 mg/L) in the region.

2. Material and methods

2.1 Study area

95

96

97

98

99

100

101

102

103

104

105

106

107

108

109

110

111

112

113

114

115

116

117

118

119

120

121

The PRE and its adjacent shelf waters (Fig. 1a) represent an estuarine system under intensive human activities. One major anthropogenic impact in the PRE is the terrestrial substances fed by the Pearl River, which is the third largest river in China

with an average annual runoff of 3.26×10¹¹ m³/ Year (Luo et al., 2002), through eight river outlets, including Humen, Jiaomen, Hongqili, Hengmen, Modaomen, Jitimen, Hutiaomen, and Yamen (Fig. 1a). The long-term DO and water quality data used here were collected from open sources (e.g. government websites) and published studies (detailed in Data availability and Table S1 of Supplement). Over the past few decades, the terrestrial inputs from the Pearl River have experienced remarkable changes in oxygen content, sediment loads, and nutrients including dissolved inorganic nitrogen (DIN) and dissolved inorganic phosphorus (DIP) (Fig. 1c-f). Consequently, the ecological environments of the PRE have changed significantly.

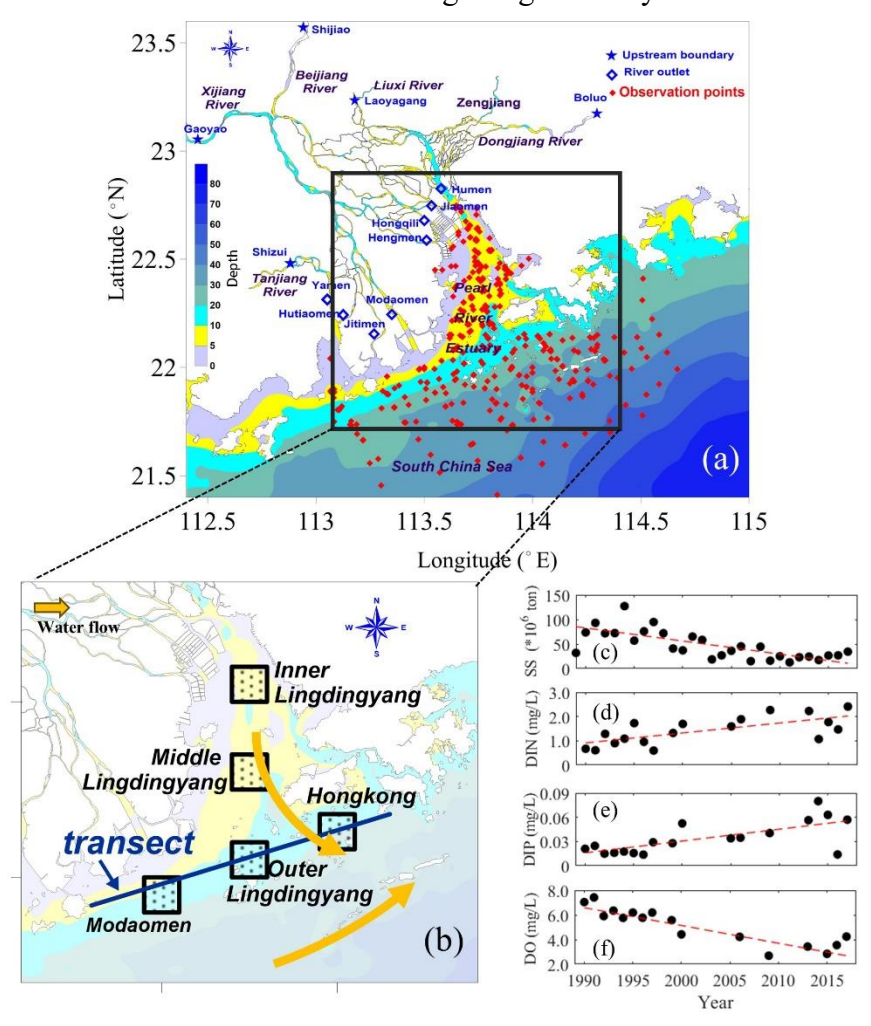


Fig. 1. (a) Study area of the PRE and sampling sites during 1985-2017; (b) five subregions and a transect along the coastal transition zone used for analysis and the water flow direction in the surface water; (c) annual loads of suspended sediments (SS) from the Pearl River; (d-f) the surface-layer (within the upper 2 m of water column) summertime concentrations of nutrients (DIN, DIP) and dissolved oxygen (DO) in the

river outlets of the PRE.

In the 1990s, the PRE displayed a low level of eutrophication levels, reflecting limited upstream urbanization at that time. This period also witnessed extensive construction of water infrastructure projects, mostly completed around 2000_(Zhang et al., 2008), which led to a dramatic reduction in the riverine suspended sediment concentration (SSC). By the late 1990s, the Pearl River basin contained at least 8636 reservoirs (Wu et al., 2016). After the 2000s, with the acceleration of urbanization and construction of hydraulic facilities, the PRE has undergone a significant increase in nutrients and decline in sediment loads (Fig. 1c-e), both of which are favorable for phytoplankton blooms and therefore for eutrophication and hypoxia. These long-term variations of riverine substances have also been reported by Lai et al. (2022) and Hu et al. (2021). In the meantime, the oxygen content in the PRE has exhibited a notable drawdown with significant expansions in low-oxygen extents in recent summers (Fig. 2), which has been revealed by the cruise observations in the PRE (Li et al., 2021; Su et al., 2017; Hu et al., 2021; Lu et al., 2018).

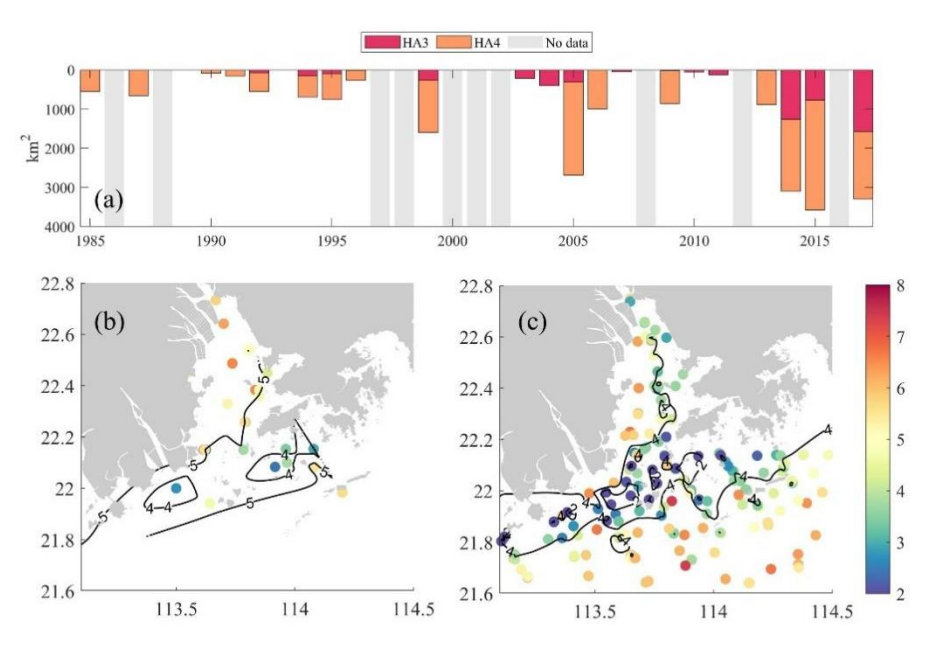


Fig. 2. (a) Interannual variations of low-oxygen area (HA4, DO \leq 4 mg/L) and hypoxic area (HA3, DO \leq 3 mg/L) in the bottom waters (\sim 1-2 m above sediments) of the PRE during summer estimated from the cruise observations (note that the grey patches represent the lack of data); spatial distributions of summer-averaged DO concentrations

160

161

162

163

164

165

166

167

168

169

170

171

172

173

174

175

176

177

178

179

180

181

182

183

184

2.2 Model settings and validation

2.2.1 Model descriptions and settings

An online 1D-3D coupled physical-biogeochemical model, which has been extensively verified and applied in the PRE (Wang et al., 2017; Wang et al., 2018; Hu et al., 2011; Zhang et al., 2022), was utilized here to reproduce the oxygen dynamics under the long-term changes in riverine nutrients, suspended sediment concentration (SSC), and oxygen content (Fig. 1c-f). This 1D-3D modeling framework integrates a 1D representation of the Pearl River network with a 3D simulation of the Pearl River Estuary and adjacent shelf region, operating in an offline coupling mode. The 1D component numerically solves the Saint-Venant equations using a Preissmann scheme, discretizing the river network into 299 sections with five upstream boundaries (specified as either discharge or water level inputs). The 3D component employs the ECOM model with 16 vertical layers and adaptive horizontal resolution (400m to 3km), forced by tides, atmospheric forcing, and open boundary conditions. The two components exchange fluxes at eight river outlets: the 3D model incorporates river discharge from the 1D model as upstream boundary conditions, while the 1D model uses water levels computed by the 3D model as its downstream boundaries at each time step. This 1D-3D modeling framework was initially developed to investigate nutrient fluxes to the PRE and has been extended and validated to simulate oxygen dynamics and hypoxia in the PRE (Wang et al., 2017; Wang et al., 2018; Hu et al., 2011; Zhang et al., 2022; Chen et al., 2024). For the sake of conciseness in the main text, detailed descriptions on the physical and suspended sediment modules were provided in the Supplement (Text S1). Regarding the biogeochemical module, it is based on the Row-Column Aesop (RCA), which simulates interactive cycles of oxygen, carbon, nitrogen, phosphorus, and silicon in the water column (Fizpartick, 2004). As for the oxygen dynamics, it can be described as follows:

185
$$\frac{\partial DO}{\partial t} = -\mathbf{u} \cdot \nabla DO + \nabla \cdot (\mathbf{D}\nabla DO) + Rea + Phot + WCR + SOD$$
 (1)

- where the velocity vector u = (u, v, w), ∇DO represents the gradient operator (spatial
- derivative of dissolved oxygen concentration), and D is the diffusion coefficient tensor.;
- 188 Rea and Phot, WCR, and SOD represent the rates of air-water oxygen exchange,
- photosynthesis, water column respiration, and sediment oxygen demand, respectively
- 190 (unit: mg O₂ L⁻¹ day⁻¹). The air-water oxygen exchange is parameterized as:

$$191 Rea = K_a \theta_a^{T-20} \cdot (DO_{sat} - DO) (2)$$

- where K_a is the surface mass transfer coefficient (m/day), θ_a is the temperature
- 193 coefficient, T is the water temperature, and DO_{sat} is dissolve oxygen saturation
- 194 concentration. The SOD is calculated by the sediment flux module (SFM) coupled to
- the RCA. The sediment module simulates the sedimentation and remineralization of
- organic carbon, nitrogen, and phosphorus, and dynamically estimates the oxygen and
- nutrient fluxes across the sediment-water interface (Fizpartick, 2004).
- The growth of phytoplankton is co-limited by temperature, light, and nutrient
- 199 conditions. The calculation of gross primary production (GPP, mg C L⁻¹ day⁻¹) of
- 200 phytoplankton is determined as:

201
$$GPP = G_{Pmax} * e^{-\beta(T_{opt}-T)^2} * G_N(N) * G_I(I) * P_C$$
 (3)

- where G_{Pmax} is the maximum grow rate of phytoplankton at the optimum temperature
- 203 (day⁻¹); T_{opt} is the optimum temperature (°C); β is the shaping coefficients; T is the
- water temperature (°C); $G_I(I)$ is the light limitation factor; $G_N(N)$ is the nutrient
- limitation factor; P_c is the phytoplankton biomass (mg C L⁻¹).
- The nutrient limitation factor $(G_N(N))$ is parameterized as:

$$207 G_N(N) = Min\left(\frac{DIN}{K_{mN} + DIN}, \frac{DIP}{K_{mP} + DIP}, \frac{Si}{K_{mSi} + Si}\right) (4)$$

- where DIN, DIP, and Si represent the concentration (mg L⁻¹) of dissolved inorganic
- 209 nitrogen (including NO₃⁻ and NH₄⁺), dissolve inorganic phosphorus (PO₄³⁻), and
- dissolve inorganic silicon (SiO₃²⁻), respectively; K_{mN} , K_{mP} , and K_{mSi} represent the
- 211 half-saturation constants (mg L⁻¹) for DIN, DIP, and Si, respectively. It should be noted

- that a higher nutrient limitation factor $G_N(N)$ indicates a weaker nutrient limitation
- 213 effect on phytoplankton growth. Moreover, the nitrogen and phosphorus limitation are
- 214 more significant than silicon limitation within the PRE, thus this study mainly focuses
- on the former.
- The light limitation factor $G_I(I)$ is parameterized as:

217
$$G_I(I) = \frac{e}{k_e H} \left[\exp\left(\frac{-I_0(t)}{I_S} e^{-k_e H}\right) - \exp\left(\frac{-I_0(t)}{I_S}\right) \right]$$
 (5)

$$218 k_e = k_{ebase} + k_c * a_{cchl} * P_c + k_{sed} * SSC + k_{POC} * POC$$
 (6)

$$219 I_0 = I_{surf} * e^{-k_e * H} (7)$$

- where H is the depth of water column (m); I_0 is the incident light intensity at the
- segment surface (ly day⁻¹); I_s is the saturating light intensity (ly day⁻¹); k_e is the light
- extinction coefficient (m⁻¹); k_{ebase} is the background light extinction coefficient of
- water (m⁻¹); k_c is the phytoplankton-related extinction coefficient (m² mg⁻¹ Chla); a_{cchl}
- 224 is the ratio of chlorophyll to phytoplankton carbon biomass; k_{sed} is the SSC-related
- extinction coefficient (m² mg⁻¹ SSC); k_{POC} is the POC-related light extinction
- coefficient (m 2 mg $^{-1}$ POC); I_{surf} is the instantaneous light radiation received at the
- water surface (ly day⁻¹).

- To estimate the spatial characteristics of light conditions, we also calculated the
- eutrophic depth in the PRE (H_E , Equation 8), which is defined as the water depth
- reached by 1% of the surface light intensity (I_{surf}) . Basically, a larger eutrophic depth
- indicates a better light condition for phytoplankton growth.

232
$$I_{surf} * e^{-k_e * H_E} = I_{surf} * 1\%$$
 (8)

233 where H_E represents the eutrophic depth (m).

2.2.2 Model validation

- The coupled physical-biogeochemical model mentioned above has already been
- validated against a variety of observations for several periods, which showed good
- 237 performance in reproducing the physical conditions, suspended sediment dynamics,
- and biogeochemical cycles in the PRE. We briefly summarized the validation results
- here. For the physical and suspended sediment modules, Hu and Li (2009) has applied

the 1D-3D coupled model to establish 30-day realistic simulations for July 1999 and February 2001. The simulated water levels, discharges, salinity, and SSC agreed well with the observations in the Pearl River network and the PRE for both periods, with correlation coefficients all greater than 0.65 in summer. The simulated SSC at the surface was also compared to satellite remote sensing data, which showed a fairly close spatial pattern and comparable concentration magnitude. Furthermore, Wang et al. (2017) provided an extensive model validation using field data collected from four seasonal cruises in 2006, with high correlations for water levels (> 0.95), salinity (> 0.90) and temperature (> 0.80) and low root-mean-standard-errors between the simulation and observations in summer.

240

241

242

243

244

245

246

247

248

249

250

251

252

253

254

255

256

257

258

259

260

261

262

263

264

265

266

267

Then, the biogeochemical module was established and used to explore the nutrient and oxygen dynamics off the PRE in July 1999 and January-December 2006 (Hu and Li, 2009; Wang et al., 2017). The point-to-point comparisons with the water quality profiles indicated that the biogeochemical module was robust to reproduce the spatial distributions of ammonia, nitrate, phosphorus, oxygen, and chlorophyll a in the PRE. Our model demonstrated strong validation performance by accurately capturing the observed temporal expansion of hypoxia, transitioning from localized bottom hypoxia in the 1990s (Fig. 2b-c) to widespread occurrences in the 2010s (Fig. 5d-e). Initial validation against 1994-1999 summer observations showed close agreement, with simulated low-oxygen (HA4=1179.7 km²) and hypoxic (HA3=211.3 km²) areas matching observational estimates (802±437 km² and 131±84 km²; Fig. 2a, Table 3). For the 2013-2017 period, the model successfully replicated hypoxia intensification, as evidenced by HA4 expansion to 2925.5 km² aligning with observed 2715±1068 km². Projections to the 2020s indicated HA3 doubling to 617.2 km², remaining within observational uncertainty ranges (901±591 km²; 2013-2017 data), confirming the model's robustness in simulating both historical patterns and emerging hypoxia dynamics. In addition, Wang et al. (2017) has compared the simulated oxygen kinetic terms (including the air-sea re-aeration rate, water-column respiration and production rates, and sediment oxygen demand) with observations in summer, which demonstrated the model's capability in representing the important oxygen source-sink processes (e.g., oxygen consumptions across the sediment-water interface) in the PRE. Detailed model settings and parameters can be found in Wang et al. (2017).

2.3 Model experiments

268

269

270

271

272

273

274

275

276

277

278

279

280

281

282

283

284

285

286

287

288

289

290

291

292

293

294

Based on the well-validated model run in 2006 (Wang et al., 2017), the present study performed diagnostic simulations for two representative periods, characterized by low nutrients and high suspended sediments and oxygen content during 1991-1996 (referring as to the "1990s case"; Table 1) versus high nutrients and low suspended sediments and oxygen content during 2013-2017 (referring as to the "2010s case"). Each case was run from 1 January to 31 August, driven by climatological physical conditions (freshwater discharges and wind speeds detailed in Text S1 of the Supplement) averaged over 1990-2017 and by mean observed values of riverine water quality components in the corresponding period. Specifically in summertime (a period used for formal analysis here), the riverine concentrations were set to 1.0 mg/L (DIN), 0.02 mg/L (DIP), and 6.5 mg/L (DO) in the 1990s case, while they were set to 2.0 mg/L, 0.065 mg/L, and 3.5 mg/L in the 2010s case (Table 1). The riverine SSC was specified at 40 mg/L in the 2010s according to the in-situ observation near the Humen outlet in 2015 summer (Chen et al., 2020), and was set to 100 mg/L in the 1990s based on the ratio of the sediment loads between the 1990s and the 2010s (2.5 times). Long-term monitoring at river outlets showed no significant temporal trend in COD compared to the marked increases in nutrients and decreases in DO, indicating stable oxygenconsuming OM inputs. We therefore maintained constant OM concentrations between study periods (organic carbon: 2 mg/L; organic nitrogen: 0.2 mg/L; organic phosphorus: 0.03 mg/L), consistent with published historical observations (Wang et al., 2018). Furthermore, three additional model scenario simulations were conducted in order to disentangle the individual impact of each varying riverine input on the summer

deoxygenation off the PRE. The setting of each scenario was identical to that of the 1990s case except that the riverine nutrients, SSC, and DO were separately replaced by the representative value in the 2010s (referring as to the "High-nutrient case", "Low-SSC case", and "DO-restore case", respectively; Table 1)

Table 1. Riverine inputs (in unit of mg L-1) for model experiments.

Cases	DIN	DIP	DO	SSC
1990s	1.0	0.020	6.5	100
2010s	2.0	0.065	3.5	40
High-nutrient	2.0	0.065	6.5	100
Low-SSC	1.0	0.020	6.5	40
DO-restore	2.0	0.065	6.5	40

3. Results

3.1 Responses of eutrophication to human-induced changes in the PRE

3.1.1 Long-term variations in water quality distributions

To examine changes in eutrophication (a key process affecting DO dynamics) and its influential factors during summer in the PRE, we compared the simulated distributions of SSC, nutrients, Chl *a*, and POC in the surface waters between the 1990s and the 2010s cases (Fig. 3) as well as their vertical integrations in subregions (Table 2). Model results showed that the surface SSC within the PRE largely declined during the two periods. In the 1990s, SSC maintained at a high level in the inner Lingdingyang Bay (see its location in Fig. 1b), ranging from 70.0 to 100.0 mg/L (Fig. 3a). Due to the particle sinking as waters advected downstream, SSC decreased to ~10.0 mg/L in the lower reaches of the PRE in the 1990s. While in the 2010s, the riverine sediment loads have remarkably decreased, resulting in a corresponding drawdown in SSC downstream (Fig. 3b-c). Overall, the vertically-integrated SSC content in the inner Lingdingyang Bay and lower PRE dropped by 56.1% and 45.6%-47.3% to 244.5 mg/m²

and 38.4-69.2 mg/m², respectively (Table 2).

In terms of nutrients, the variation induced by riverine inputs was also evident during the two periods, acting on the main estuary in association with the spreading of the river plume. As shown, the DIN content in the 1990s was mostly below 1.5 mg/L within the entire PRE (Fig. 3d). With respect to the 2010s, the DIN concentration has increased by 0.8 mg/L and 0.2 mg/L in the surface waters of the upper Lingdingyang Bay and the lower PRE, respectively (Fig. 3e-f). The vertically-integrated DIN mass has increased by 41.9%-102% in the PRE (Table 2). A similar situation occurred with respect to DIP, with its content increasing from 0.04 mg/L in the 1990s to 0.07 mg/L in the 2010s in the high-DIP area adjacent to the middle Lingdingyang Bay (Fig. 3g-i). In terms of vertical integration, DIP increased by 9%-108%, with the lowest increases located in the Hong Kong waters downstream of the estuary (Table 2).

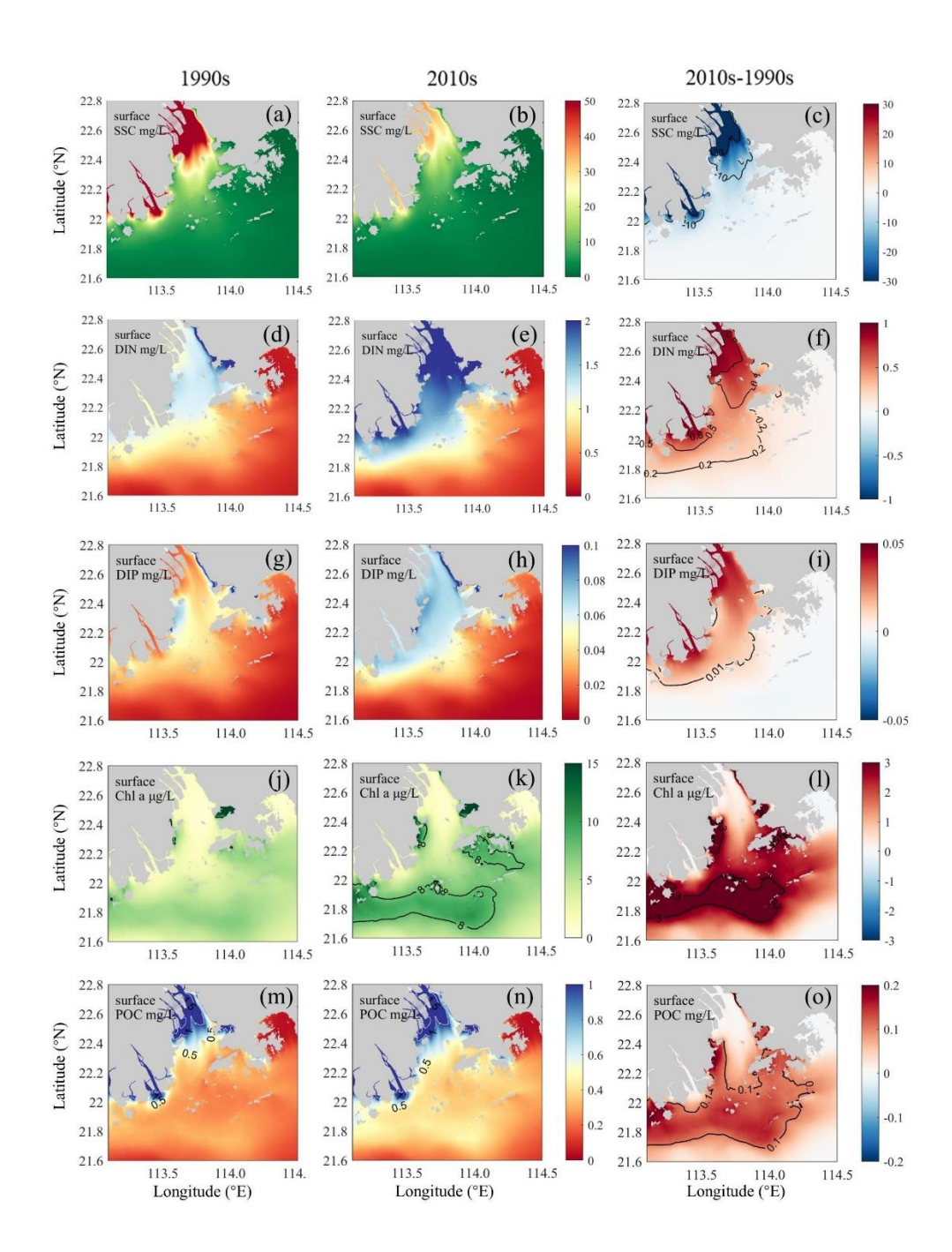


Fig. 3. Simulated distributions of (a-c) SSC, (d-f) DIN, (g-i) DIP, (j-l) Chl a, and (m-o) POC concentrations in the surface waters of the PRE for the 1990s (left panels) and the 2010s (middle panels) as well as their differences (right panels).

Table 2. Vertical integrations of DIN, DIP, SSC, Chl a, and POC contents; nutrient limitation index and euphotic depth; and DO concentrations, low-oxygen frequency (HF4), hypoxia frequency (HF3), and oxygen consumption rates in the bottom waters for subregions of the PRE (see locations in Fig. 1b) during the 1990s and the 2010s.

Carlos	Inner		Middle		Modaomen	en	Outer			04040
Suoregions	Lingdingyang Bay	ang Bay	Lingding	Lingdingyang Bay	sub-estuary	ury	Lingding	Lingdingyang Bay	nong n o	nong wong waters
Cases	1990s	2010s	1990s	2010s	1990s	2010s	1990s	2010s	1990s	2010s
DIN ($mg m^{-2}$)	6.58	12.24	5.42	9.20	4.89	7.62	5.17	7.92	3.62	5.14
$DIP (mg \ m^{-2})$	0.23	0.48	0.34	0.48	0.55	0.71	0.56	99.0	0.51	0.56
Nutrient limitation index 0.94	0.94	0.97	0.95	0.97	0.92	0.94	0.91	0.93	0.83	0.85
$SSC (mg m^{-2})$	556.5	244.5	332.9	164.6	120.4	63.4	127.7	69.2	9.07	38.4
Euphotic depth (m)	-1.3	-2.3	-2.0	4.2	-9.5	-11.2	-11.8	-15.2	-20.7	-21.0
$\mathrm{Chl}a~(\mu\mathrm{g~m}^{\text{-}2})$	5.0	7.1	11.7	22.9	39.4	70.4	40.7	72.9	74.3	108.9
POC (mg m ⁻²)	9.8	8.64	8.8	5.31	4.82	6:39	5.33	6.85	6.21	7.91
Bottom DO (mg L ⁻¹)	4.55	3.52	4.31	3.90	3.50	2.84	4.96	4.12	4.36	3.52
HF4	25.0%	79.7%	26.8%	65.2%	84.5%	99.1%	4.5%	49.3%	20.5%	61.1%
HF3	6.5%	27.6%	4.8%	10.1%	25.2%	56.5%	3.5%	9.1%	4.8%	21.4%
WCR (mg O_2 L ⁻¹ day ⁻¹)	-0.38	-0.45	-0.20	-0.25	-0.09	-0.11	-0.07	-0.09	-0.06	-0.07
SOD (mg O_2 L ⁻¹ day ⁻¹)	-1.72	-1.62	-0.89	-0.89	-0.24	-0.46	-0.28	-1.12	-0.91	-1.48

Note: HF4 (frequency of DO < 4 mg L $^{-1}$); HF3 (frequency of DO < 3 mg L $^{-1}$).

In response to changes in light (affected by the SSC content) and nutrient conditions, phytoplankton biomass has substantially grown in the 2010s, indicated by the increased Chl a concentration. In the 1990s, the phytoplankton biomass was at a low level, with the Chl a generally below 8.0 µg/L in the surface waters (Fig. 3j). As for the 2010s, significant phytoplankton blooms were found along the Modaomen subestuary, outer Lingdingyang Bay, and Hong Kong waters (Fig. 3k-l), with the vertically-integrated Chl a content rising by 31.0 µg/m² (by 78.7% compared to the 1990s), 32.2 µg/m² (79.1%), and 34.6 µg/m² (46.6%), respectively (Table 2). As a result of the elevated primary production, a great amount of organic matter was produced in the PRE. Spatially coupled to the growth of Chl a (Fig. 3l), the POC content has significantly increased in the 2010s, especially in the lower PRE (Fig. 3m-o), with the vertically-integrated concentration increasing by 1.5-2.0 mg/m² (by 27.4%-32.6% compared to the 1990s) over the water column (Table 2).

3.1.2 Long-term variations in nutrient and light limitations

The primary production in the PRE was controlled by the synergistic effects of nutrient and light conditions. We calculate the nutrient limitation factor and the eutrophic depth to quantify the intensity of nutrient limitation and light limitation on algae growth. It should be noted that a smaller nutrient limitation index and a shallower eutrophic depth represent a stronger nutrient limitation and a stronger light limitation, respectively. Results showed that the nutrient limitation exhibited a distinct estuary-shelf gradient, in which the Hong Kong waters experienced more severe nutrient limitation than the Modaomen sub-estuary and Lingdingyang Bay (Fig. 4a, c). Specifically, the nutrient limitation index decreased from the upper estuary (0.94) to the Hong Kong waters (0.83) in the 1990s. By contrast, the light limitation has attenuated along the river plume transport, largely ascribed to the decreased SSC (Fig. 3a-b). Compared to the Hong Kong waters, the regions adjacent to river outlets underwent more severe light limitation, shown by the eutrophic depth (Fig. 4b) increasing from the Lingdingyang Bay (1.3 m) and Modaomen sub-estuary (9.5 m) to the Hong Kong

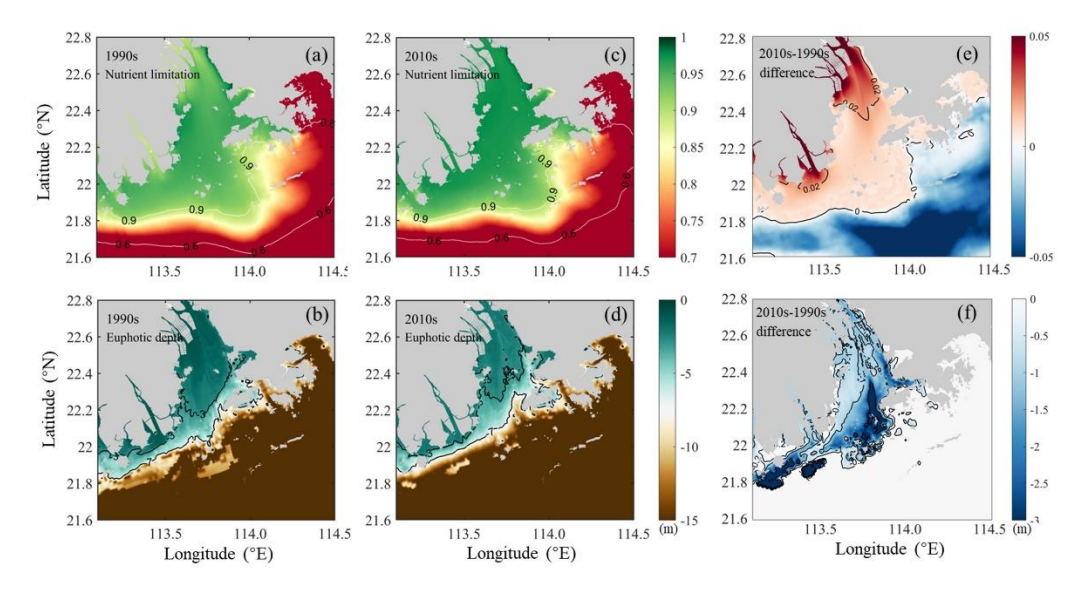


Fig. 4. Simulated distributions (a, c) and difference (e) of nutrient limitation index for the growth of phytoplankton in the 1990s and the 2010s; (b, d) euphotic depth and its difference (e) (in unit of m) in the 1990s and the 2010s.

Due to the growth in nutrient loads, nutrient limitation was relieved in the 2010s. For instance, the nutrient limitation index in the Hong Kong waters has increased to 0.85 (by 2.4% of the 1990s) in the 2010s (Table 2). In comparison, the relief of light limitation was more evident with the reduced riverine suspended sediments. The deepening of the euphotic depth in the Lingdingyang Bay was significantly greater than that in the lower estuary (Fig. 4b, d). In the inner Lingdingyang and middle Lingdingyang Bays, the euphotic depth increased by 1 m and 2.2 m (by 76.9% and 110.0% relative to the 1990s, Table2), respectively. The alterations in light conditions in the remaining area were relatively minor, with the eutrophic depth increasing to 11.2 m (by 17.9%) in the Modaomen sub-estuary and to 21 m (by 1.4%) in the Hong Kong waters during the 2010s (Table 2).

the PRE

3.2.1 Variations in DO distributions and hypoxia occurrences

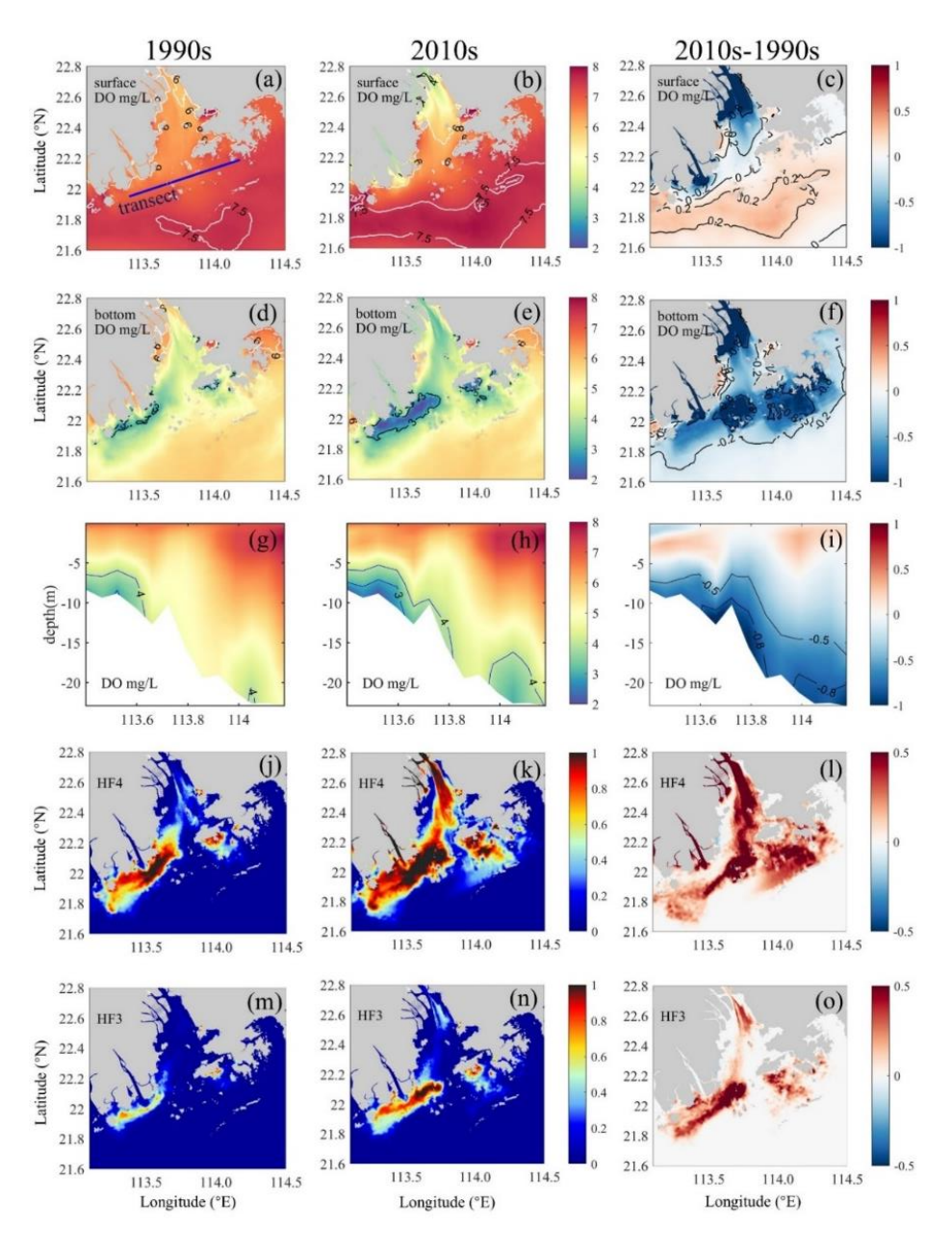


Fig. 5. (a-c) Surface DO and (d-f) bottom DO distributions, (g-i) vertical DO distributions along the transect (see its location in panel a), and (j-l) low-oxygen frequency (HF4, DO < 4 mg/L) and (m-o) hypoxia frequency (HF3, DO < 3 mg/L) in the bottom waters of the PRE for the 1990s (left panels) and the 2010s (middle panels) as well as their differences (right panels). Note that hypoxia frequency is calculated as the number of hypoxic days divided by the total number of days in the study period,

yielding a dimensionless ratio (range: 0–1).

Our model revealed distinct temporal shifts in summertime DO patterns and hypoxia distribution (Fig. 5). The surface DO in the 1990s was generally higher than 6 mg/L, increasing trend towards the shelf regions (Fig. 5a). By the 2010s, surface DO levels had increased by 0.2-0.3 mg/L (Fig. 5b-c), with an oxygen-enriched zone in the lower PRE correlating with high Chl a (Fig. 3k), though new low-oxygen zones (DO <4 mg/L) emerged near river outlets due to reduced Pearl River DO influx.

Bottom water simulations captured the hypoxia expansion from small-scale 1990s events (Fig. 2b-c) to widespread 2010s occurrences (Fig. 5d-e). Initial hypoxia clustered along the western PRE (Modaomen sub-estuary; Fig. 5d), with simulated HA4 (1179.7 km²) and HA3 (211.3 km²) (Table 3) matching observations (802±437 km² and 131±84 km²; 1994-1999 summers; Fig. 2a). By the 2010s, hypoxia intensified throughout Lingdingyang Bay and Hong Kong waters, with bottom DO declining to 2.8-4.1 mg/L (Table 2). Simulated HA4 expanded 1.5-fold to 2925.5 km² (Table 3), consistent with observed 2715±1068 km² (2013-2017; Fig. 2a). HA3 doubled to 617.2 km² by the 2020s, comparable to observed 901±591 km² (2013-2017).

Table 3. Simulated low-oxygen (HA4, DO < 4 mg/L) and hypoxic (HA3, DO < 3 mg/L) areas in the bottom waters of the PRE and their changes relative to the 1990s.

1// 051				
Cases	HA4 (km ²)	Percentage of	HA3 (km ²)	Percentage of
	11A4 (KIII)	change	IIA3 (KIII)	change
1990s	1179.7	/	211.3	/
2010s	2925.5	+148%	617.2	+192%
High-nutrient	1542.6	+31%	282.5	+34%
Low-SSC	1737.0	+47%	412.4	+95%
DO-restore	2409.7	+104%	617.2	+192%

Note: The calculation in percentage of change is: $(HA_x-HA_{1990s})/HA_{1990s}$, where x represents each case.

In addition, our model accurately replicated the two observed hypoxic centers along the coastal transition zone (Modaomen sub-estuary and Hong Kong waters; Fig.

2b-c), revealing distinct spatiotemporal deoxygenation patterns (Fig. 5g-o). During the 1990s, both centers exhibited limited low-oxygen zones, with Hong Kong waters showing <1 m thick DO <4 mg/L layers (Fig. 5g). Low-oxygen (HF4) and hypoxic (HF3) conditions persisted 18-76 days (20.5%-84.5% frequency) and 4-23 days (4.8%-25.2%) respectively during summer months (Fig. 5j,m; Table 2).

By the 2010s, hypoxic thickness increased substantially to ~1.5 m at Modaomen and ~5 m (~4 m thicker than 1990s) at Hong Kong waters (Fig. 5h). Event durations prolonged to 55-89 days (61.0%-99.1% HF4) and 19-51 days (21.4%-56.5% HF3) respectively (Fig. 5k, n; Table 2), demonstrating intensified and prolonged hypoxia.

3.2.2 Variations in bottom oxygen consumption

To further explore the mechanism of long-term deoxygenation off the PRE, we investigated the oxygen consumption rates and their changes during the two periods (the 1990s versus the 2020s). We specifically focused on the oxygen consumption at the bottom layers covering the 20% of the water depth above the sediments, where the majority of hypoxic events in the PRE occurred (Fig. 5).

As shown in Table 2, the predominant oxygen sink in the bottom waters of the

As shown in Table 2, the predominant oxygen sink in the bottom waters of the PRE was sediment oxygen demand (SOD) induced largely by the remineralization of organic matter in sediments, whereas water column respiration (WCR) only accounted for 15.2% of the bottom oxygen consumption on average. Over the past three decades, both the WCR and SOD have generally increased in the PRE, primarily attributed to the growth in local production of organic matter associated with aggravated eutrophication (Fig. 3j-o). Particularly, the SOD in the outer Lingdingyang Bay and Hong Kong waters has remarkably increased from 0.28-0.92 mg O₂ L⁻¹ day⁻¹ in the 1990s to 1.12-1.48 mg O₂ L⁻¹ day⁻¹ in the 2010s (Table 2), which contributed to 80%~95% of the increment in total oxygen consumption. Although the absolute increase of SOD in the Modaomen sub-estuary was comparatively small, the SOD in the 2010s has almost doubled compared to the 1990s, leading to a substantial increase in the

occurrence of hypoxic events in this region (Fig. 5d-o).

3.2.3 Disentangling contributions of riverine oxygen, suspended sediments, and nutrient changes on deoxygenation

As detailed in Section 2.3, three scenario simulations were performed to quantify the relative contributions of riverine changes to the decadal low-oxygen expansion in the PRE (Table 1). In general, the riverine impacts on DO and related biogeochemical factors varied significantly between subregions (Figs. 6-7). Specifically, increasing the riverine nutrient levels from the 1990s to the 2020s alone (High-nutrient case) led to a marked drawdown in the bottom DO around the lower PRE (by over 0.2 mg/L relative to the 1990s; Fig. 6a). The DO decline, extending from the Modaomen sub-estuary to the Hong Kong waters, was ascribed to the elevated phytoplankton biomass (Fig. 7b) facilitated by better nutrient conditions, which subsequently sustained stronger bottom oxygen depletions compared to the 1990s (Fig. 7c). Among the subregions, the Hong Kong waters was more susceptible to the changes in riverine nutrients as it was subject to comparatively severe nutrient limitation (Table 2). Therefore, with the improvement of nutrient utilization, this region experienced more pronounced deoxygenation in association with significant alterations in Chl a content and SOD (increased by 14.2 μg/m² and 0.26 mg O₂ L⁻¹ day⁻¹, respectively, equivalent to 47.1% and 46.4% of their total increments over the past three decades; Fig. 7). While in the inner Lingdingyang Bay, the increased nutrient inputs only caused a slight change in Chl a content because the phytoplankton growth in this region was mostly light limited due to high water turbidity (Table 2). The concomitant changes in SOD and bottom DO were fairly small as well. Collectively, the high-nutrient scenario alone resulted in a 31% and 34% growth in the area affected by low oxygen (HA4) and hypoxia (HA3) relative to the 1990s, respectively (Table 3).

445

446

447

448

449

450

451

452

453

454

455

456

457

458

459

460

461

462

463

464

465

466

467

468

469

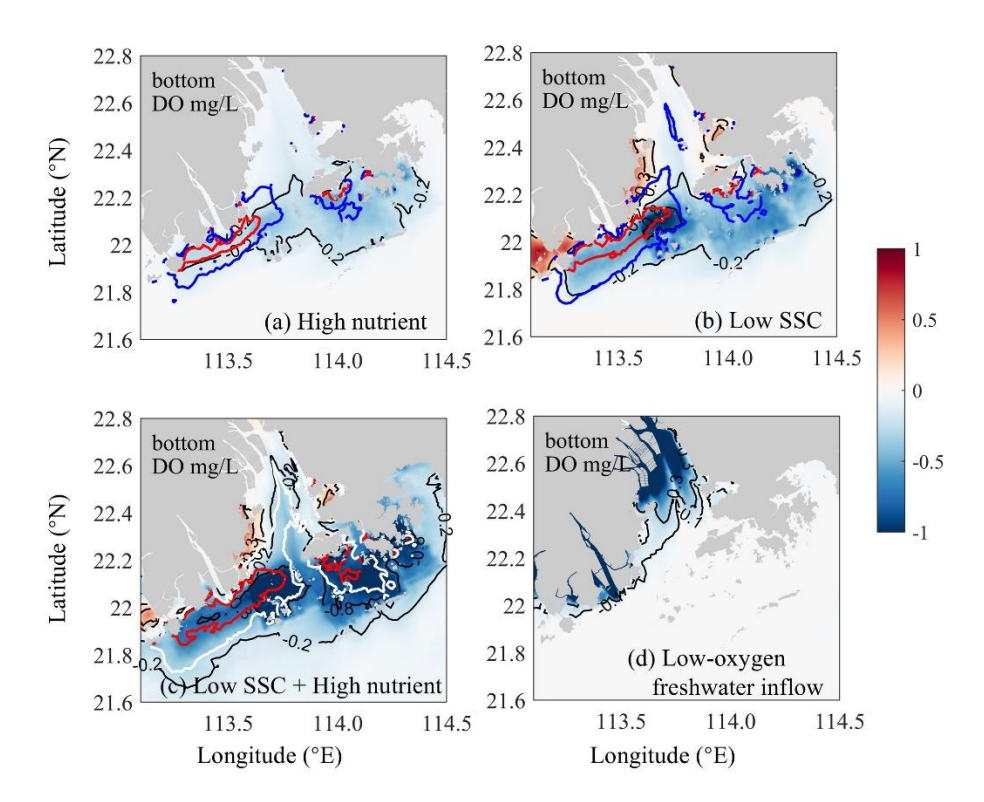


Fig. 6. Bottom DO changes induced by (a) riverine nutrient increases (the High-nutrient case minus the 1990s case), (b) riverine SSC declines (the Low-SSC case minus the 1990s case), (c) the combined effects of nutrient increases and SSC declines (the DO-restore case minus the 1990s case), and (d) riverine DO declines (the DO-restore case minus the 2010s case), respectively. The blue and white contour lines represent DO = 4 mg/L for the respective cases, and the red contour lines represent DO = 3 mg/L.

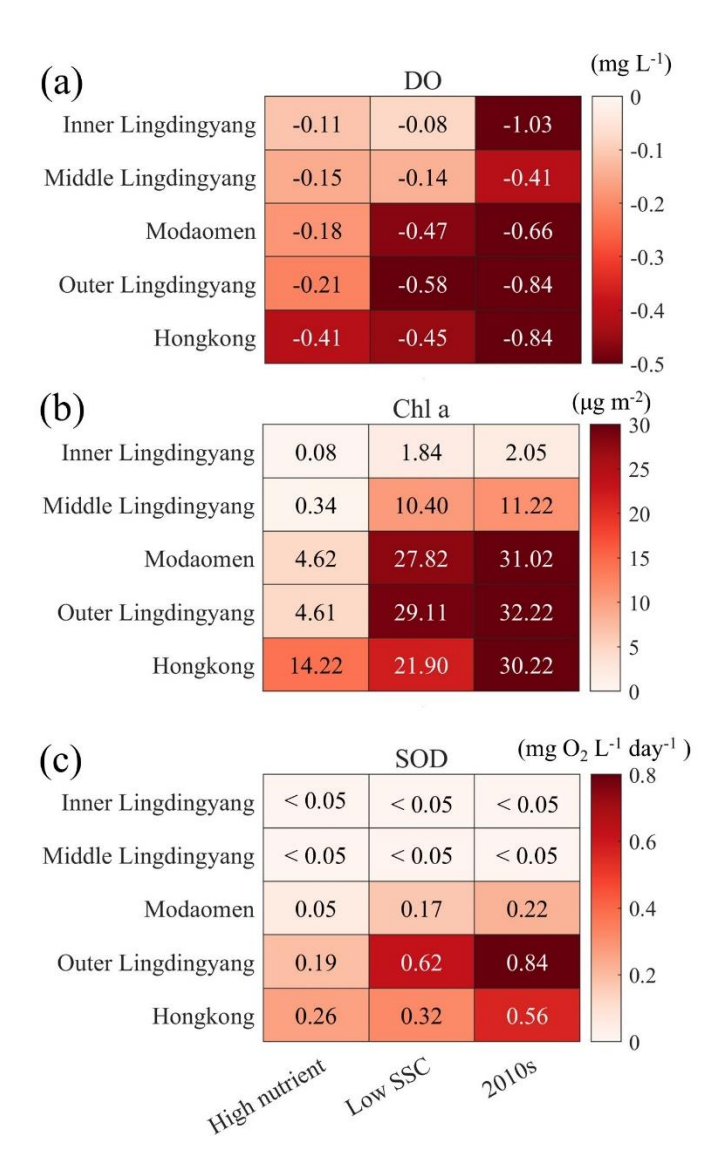


Fig. 7. Changes of (a) bottom DO concentration, (b) vertically-integrated Chl a content, and (c) SOD in subregions of the PRE for the High-nutrient, the Low-SSC, and the 2010s cases relative to the 1990s case.

Compared with the High-nutrient case, reducing the riverine suspended sediment loads from the 1990s to the 2020s alone (Low-SSC case) imposed a greater impact on the DO conditions, causing more extensive and intense deoxygenation through the PRE (Fig. 6b). Apparent DO decline (exceeding 0.3 mg/L relative to the 1990s) occurred within the lower PRE, similar to that of the changing riverine nutrients described above. This is also attributed to the intensified SOD (with an increment of 0.17-0.62 mg O₂ L⁻¹ day⁻¹, accounting for 57.1%-77.3% of the total increment during the two periods; Fig.

7c), accompanied by a prominent increase in Chl a content (by $21.9-29.1 \text{ µg/m}^2$, accounting for 72.4%-90.3% of the total increment; Fig. 7b) due to the improved light condition (the relief of light limitation; Table 2). The SSC-induced changes in these biogeochemical factors were more pronounced in the outer Lingdingyang Bay and Modaomen sub-estuary than in other regions including the Hong Kong waters, which coincided with the alterations in deoxygenation among the subregions (Fig. 7). Overall, under the low-SSC scenario the low-oxygen area (HA4) and hypoxic area (HA3) expanded by 47% and 95% compared to the 1990s, respectively (Table 3). As shown in Figure 7 and Table 3, the combined effect of reducing SSC and increasing nutrient inputs (DO-restore case) led to a significant expansion of low-oxygen conditions, with hypoxic areas (HA4) and low-oxygen areas (HA3) reaching 2409.7 km² and 617.2 km², respectively. This combined effect exceeded the sum of changes induced by individual river inputs, highlighting the non-linear interaction between SSC and nutrient loading. In regions such as Outer Lingdingyang and Hong Kong, the combined effect was amplified, while in regions such as Inner and Middle Lingdingyang, the combined effect was less than the sum of individual effects. The growth of phytoplankton is not a linear process in response to various influencing factors; instead, these factors interact cumulatively. Therefore, when different factors are combined, their combined effect can exceed the impact of individual factors acting alone.

491

492

493

494

495

496

497

498

499

500

501

502

503

504

505

506

507

508

509

510

511

512

513

514

515

516

517

518

With respect to the influence of altered riverine DO influx, it could be deduced from the difference between the 2010s and the DO-restore cases (Fig. 6d). There was a considerable DO decrease (by over 0.8 mg/L) in the bottom waters adjacent to the river outlets (also in the surface waters) owing to the low-oxygen inflows from the upstream river channels. The impact of these low-oxygen waters was largely restricted within the upper Lingdingyang Bay under the effects of air-sea reoxygenation and water-column mixing along with the river plume transport. Collectively, reducing the riverine DO content from the 1990s to the 2020s alone resulted in an enlargement of low-oxygen area by nearly 515.8 km² (derived by subtracting the HA4 of the 2010s case from that

4. Discussion

519

520

521

522

4.1 Impacts of decadal changes in riverine inputs on

deoxygenation off the PRE

523 By integrating long-term observations with physical-biogeochemical model simulations, we revealed significant bottom-water deoxygenation in the Pearl River 524 525 Estuary over the past three decades, driven by changes in riverine inputs. From the 526 1990s to 2020s, summer inflows of DIN and DIP increased by ~100% and ~225%, 527 while SSC decreased by ~60% due to human activities like dam construction (Liu et al., 528 2022) and reforestation (Cao et al., 2023). Concurrently, oxygen depletion from terrestrial pollutants reduced riverine DO concentrations by 46% (Ma et al., 2024). 529 530 These shifts collectively intensified bottom-water low-oxygen conditions in PRE (Fig. 531 5), with model simulations showing a 148% expansion in summer low-oxygen areas 532 (DO < 4 mg/L) and a 192% decrease in hypoxic areas (DO < 3 mg/L). Low-oxygen 533 events also become more persistent, lasting longer (~15-35 days during June-August) 534 and expanding vertically by \sim 1-4 m and (Table 3). 535 More interestingly, the PRE has developed three distinct hypoxic centers (including the inner Lingdingyang Bay, Modaomen sub-estuary, and Hong Kong waters) 536 537 controlled by different dominant factors, which renders the deoxygenation problem in 538 this region as a great reference for estuaries and coastal systems worldwide. Specifically, 539 the impact of riverine low-oxygen waters was confined within the upper estuary close 540 to the river outlets, leading to a ~44% increase in the low-oxygen area relative to the 541 1990s. Such local low-oxygen issue could be mitigated to a large extent if the riverine DO recovered to a comparatively higher level (e.g., ~6.5 mg/L in the 1990s) according 542 543 to the DO-restore scenario (Fig. 6d). Reduced water turbidity downstream facilitates 544 the upstream transport of nutrients, promoting eutrophication and oxygen depletion in

the lower reaches, which is highly sensitive to changes in riverine nutrient and sediment inputs. As indicated in the High-nutrient and the Low-SSC cases, the increased nutrient inputs and declined suspended sediment loads have separately alleviated the nutrient and light limitations on algae growth in the region, thereby stimulating phytoplankton blooms and local production of organic matter to support subsurface oxygen consumption (dominated by sediment oxygen uptake, SOD; Fig. 7).

While previous studies have primarily examined the impacts of riverine inputs of freshwater, nutrients and organic matter, this study provides a comprehensive investigation of how suspended sediment reduction influences estuarine dissolved oxygen dynamics. In the PRE, the riverine SSC reduction played a more important role in driving the long-term low-oxygen expansion. Its synergistic effect with the riverine nutrient changes could further amplify the exacerbation of eutrophication and subsequent deoxygenation, resulting in an enlarged growth in the low-oxygen area (by 104%) and hypoxic area (by 192%) that was notably larger than the total of their partial contributions (Table 3), and reached 70% of the total impact from combined SSC, nutrient, and low-oxygen changes (148% low-oxygen expansion).

It is worth mentioning that the relative importance of the riverine nutrient and SSC changes were different between the two hypoxic centers in the lower PRE, depending upon their distances and water flow conditions from the river outlets. Closer to the river outlets, the Modaomen sub-estuary and its surrounding waters (located on the western side of the coastal transition zone off the PRE) possessed a fairly high SSC level, which imposed a stronger light limitation on the growth of phytoplankton in the region, ultimately making the oxygen dynamics more susceptible to the decline in riverine SSC. Suspended sediments were confined to the coastal area of Modaomen by water currents (Fig. 1b), resulting in a significant decrease in sediment deposition in this region, which greatly improved light availability, ultimately making the oxygen dynamics more susceptible to the decline in riverine SSC. On the contrary, the Hong Kong waters and adjacent coastal areas (located on the eastern side of the coastal transition zone) far

from the river outlets were less affected by the riverine inputs, where the relatively low nutrient levels promoted more sensitive responses of biogeochemical processes (e.g. primary production and SOD) and hypoxia occurrences to nutrient variations. Besides, the complex island topography near Hong Kong (Fig1b) creates hydrodynamic barriers that restrict the offshore transport of suspended sediments.

4.2 Nutrient control and hypoxia mitigation in the context of

sediment declines

573

574

575

576

577

578

579

580

581

582

583

584

585

586

587

588

589

590

591

592

593

594

595

596

597

598

599

Our results underscored the substantial spatial variability in the regulation of riverine inputs on deoxygenation, highlighting the need for more refined and targeted strategies for hypoxia mitigation. Compared with the riverine nutrients, the regulatory effects of SSC on eutrophication and hypoxia have received less attention. This oversight suggests that previous studies may have overestimated nutrient impacts when failing to account for SSC-mediated processes required to align model simulations with observed deoxygenation patterns. Such model overcompensation could lead to potentially optimistic assessments of hypoxia mitigation effectiveness under proposed nutrient control plans. It is therefore critical to disentangle and quantitatively reevaluate the relative contributions of riverine nutrients versus SSC changes to coastal deoxygenation dynamics over recent decades. As demonstrated in the PRE case study, the current low-SSC regime suggests more stringent nutrient reductions than previously estimated might be required to effectively curb deoxygenation. Furthermore, it should be noted that although the dam constructions in the Pearl River Basin have mostly completed since the 2000s, it is still unclear whether the declining trend of riverine SSC will persist in the future. For instance, the reforestation in recent years has shown to be effective in reducing the summer freshwater discharges and sediment loads in the Pearl River Basin (Cao et al., 2023). This evolving context underscores that SSC variations will continue to play a defining role in future oxygen dynamics, introducing compounding uncertainties for hypoxia mitigation strategies. Notably, analogous

sediment-oxygen coupling mechanisms are emerging in other hypoxic systems. For example, it was reported that the decrease of riverine SSC (by ~56%) appeared to be the predominant factor for the intensifying eutrophication (with a 61% increase in the Chl a concentration) in the Yangtze River Estuary over the past decades (Wang et al., 2019). In addition, several modelling studies have showed that the dam constructions in the upper regions of Guadiana Estuary have significantly reduced the water turbidity and exacerbated eutrophication in the lower estuary (Domingues et al., 2012; Barbosa et al., 2010). A global-scale survey revealed that the sediment loads in 414 major rivers has approximately decreased by 51% since the 2000s due to human activities (Dethier et al., 2022), suggesting that the deteriorating eutrophication and deoxygenation in the context of sediment declines has become a global concern and merits more attention and investigations in the future. While our study emphasizes the impacts of reduced suspended sediments, human activities may conversely increase sediment loads in estuaries. For example, land-use changes such as deforestation (Kasai et al., 2005) or industrialization (Syvitski and Kettner, 2011) may exacerbate soil erosion and sediment transport, leading to higher suspended sediment concentrations in the water. In such cases, light attenuation due to increased turbidity may suppress phytoplankton growth and reduce primary production, thereby mitigating hypoxia.

600

601

602

603

604

605

606

607

608

609

610

611

612

613

614

615

616

617

618

619

620

621

622

623

624

625

626

627

Some caveats to our work require further studies. First, our light attenuation parameterization builds upon the empirical formulation of Ditoro (2001), previously validated for the Pearl River Estuary (PRE) through biogeochemical consistency checks (Wang et al., 2018). While this approach successfully captured observed oxygen dynamics in our simulations, two key simplifications require explicit discussion. The current light attenuation parameterization in our model primarily accounts for the effects of chlorophyll and suspended sediments. Previous studies have demonstrated that CDOM (colored dissolved organic matter) also plays a significant role in light attenuation within the PRE (Cao et al., 2003; Wang et al., 2010), particularly during algal bloom periods. Although our model does not explicitly treat CDOM as an

independent variable, its influence is indirectly accounted for within the existing parameterization. However, to accurately quantify CDOM's contribution to oxygen dynamics—including its long-term trends—future work should incorporate an explicit representation of CDOM's effects on light attenuation in the model, alongside sustained observational monitoring of CDOM. Apart from anthropogenic activities, alterations in regional physical conditions aligning with climate changes such as wind and freshwater discharge could also regulate the long-term deoxygenation in coastal regions (Yu et al., 2015; Chen et al., 2024). Besides, the impacts of ocean warming on deoxygenation (Laurent et al., 2018) remain unclear in the PRE as well, although warming has already been observed in the PRE (Cheung et al., 2021). Its compounding factors such as sealevel rise (Hong et al., 2020) may introduce additional complexity to hypoxia evolution through cascading ecosystem effects. While these factors have not been considered in this study, the relative contributions of human activities and climate changes represent a significant topic for future investigations, which can facilitate a more comprehensive understanding of oxygen dynamics and hypoxia development in estuaries and coastal systems.

5. Conclusion

628

629

630

631

632

633

634

635

636

637

638

639

640

641

642

643

644

645

646

647

648

649

650

651

652

653

654

We applied a well-validated physical-biogeochemical model to reconstruct the summertime oxygen distributions in the PRE during two representative periods (the 1990s and the 2010s) and to disentangle the contribution of alterations in riverine inputs (i.e., suspended sediments, nutrients, and oxygen concentration) to the long-term deoxygenation off the PRE based on a suite of model experiments. We found that owing to the changes of riverine inputs over the past three decades, the low-oxygen and hypoxic areas in the bottom waters of the PRE have expanded by about 1.5 times and two-fold, respectively, with the duration time prolonged by ~15-35 days in summer. Concurrently, three hypoxic centers dominated by distinct factors were identified. Scenario simulations revealed that the decline in riverine oxygen concentration has

caused a low-oxygen expansion (by ~44%) in the upper PRE. By comparison, the alterations in riverine nutrients and suspended sediments have separately provided better nutrient and light conditions to promote higher production of labile organic matter, which jointly maintained considerable oxygen depletions and exacerbated the low-oxygen conditions in the lower PRE. The relative importance of the changing riverine nutrients and suspended sediments to deoxygenation varied between subregions. The suspended sediment reduction was the predominated factor in the downstream regions close to the river outlets (e.g. the Modaomen sub-estuary), while the nutrient increase exerted a more substantial influence in the regions far from the river outlets (e.g. the Hong Kong waters). Our study highlights the significant role of the declined suspended sediments in the low-oxygen expansion off the PRE, which can further amplify the effect in association with the increasing nutrients. Therefore, in the context of global regimes changes of riverine suspended sediments, we call for an urgent re-evaluation of the impacts of riverine inputs on deoxygenation in addition to nutrients in order to better understand the mechanism controlling hypoxia and thereby proposing effective mitigation strategies.

671

672

677

678

679

680

681

655

656

657

658

659

660

661

662

663

664

665

666

667

668

669

670

CRediT authorship contribution statement

- Yue Nan: Investigation, Model experiments, Formal analysis, Visualization,
- Writing-original draft. **Zheng Chen:** Model experiments, Writing-review. **Bin Wang:**
- 675 Writing-review. Bo Liang: Writing-review. Jiatang Hu: Project administration,
- 676 Supervision, Conceptualization, Writing-review & editing.

Declaration of competing interest

The authors declare that they have no known competing financial interests or personal relationships that could have appeared to influence the work reported in this paper.

Acknowledgements

This work was supported by a grant from the Southern Marine Science and Engineering Guangdong Laboratory (Zhuhai) (Project. SML2023SP220) and two consulting projects (ZB-2023-005, ZB-2023-054) to JH.

Data availability

 The dissolved oxygen observation datasets off the Pearl River Estuary were obtained from published studies (Hu et al., 2021, DOI: 10.5194/bg-18-5247-2021; Su et al., 2017, DOI: 10.5194/bg-14-4085-2017; Li et al., 2021, DOI: 10.1029/2020JC016700) and the Hong Kong Environmental Protection Department (www.epd.gov.hk). The observed nutrients, oxygen, and suspended sediments data in the Pearl River are available from Hu et al. (2021) and publicly accessible databases maintained by China's Ministry of Ecology and Environment (https://www.mee.gov.cn/) and the China River Sediment Bulletin (http://www.mwr.gov.cn/sj/tjgb/zghlnsgb/).

695 Reference

- 696 Barbosa, A. B., Domingues, R. B., and Galvão, H. M.: Environmental Forcing of
- 697 Phytoplankton in a Mediterranean Estuary (Guadiana Estuary, South-western Iberia):
- 698 A Decadal Study of Anthropogenic and Climatic Influences, Estuaries and Coasts, 33,
- 699 324-341, 10.1007/s12237-009-9200-x, 2010.
- 700 Bianchi, T. S., DiMarco, S. F., Cowan, J. H., Hetland, R. D., Chapman, P., Day, J. W.,
- and Allison, M. A.: The science of hypoxia in the Northern Gulf of Mexico: A review,
- 702 Science of The Total Environment, 408, 1471-1484,
- 703 https://doi.org/10.1016/j.scitotenv.2009.11.047, 2010.
- 704 Breitburg, D., Levin, L. A., Oschlies, A., Grégoire, M., Chavez, F. P., Conley, D. J.,
- Garçon, V., Gilbert, D., Gutiérrez, D., Isensee, K., Jacinto, G. S., Limburg, K. E.,
- Montes, I., Naqvi, S. W. A., Pitcher, G. C., Rabalais, N. N., Roman, M. R., Rose, K. A.,
- Seibel, B. A., Telszewski, M., Yasuhara, M., and Zhang, J.: Declining oxygen in the
- global ocean and coastal waters, Science, 359, eaam7240, 10.1126/science.aam7240,
- 709 2018.
- 710 Bussi, G., Darby, S. E., Whitehead, P. G., Jin, L., Dadson, S. J., Voepel, H. E.,
- 711 Vasilopoulos, G., Hackney, C. R., Hutton, C., Berchoux, T., Parsons, D. R., and
- 712 Nicholas, A.: Impact of dams and climate change on suspended sediment flux to the
- 713 Mekong delta, Science of The Total Environment, 755, 142468,
- 714 https://doi.org/10.1016/j.scitotenv.2020.142468, 2021.
- 715 Cao, W., Yang, Y., Xu, X., Huang, L., and Zhang, J.: Regional patterns of particulate
- spectral absorption in the Pearl River estuary, Chinese Science Bulletin, 48, 2344-2351,
- 717 2003.
- 718 Cao, Z., Duan, H., Ma, R., Shen, M., and Yang, H.: Remarkable effects of greening
- 719 watershed on reducing suspended sediment flux in China's major rivers, Science
- 720 Bulletin, 68, 2285-2288, 2023.
- 721 Carstensen, J., Andersen, J. H., Gustafsson, B. G., and Conley, D. J.: Deoxygenation of
- the Baltic Sea during the last century, Proceedings of the National Academy of Sciences
- 723 of the United States of America, 111, 5628-5633, 10.1073/pnas.1323156111, 2014.
- 724 Chen, J. Y., Pan, D. L., Liu, M. L., Mao, Z. H., Zhu, Q. K., Chen, N. H., Zhang, X. Y.,
- 725 and Tao, B. Y.: Relationships Between Long-Term Trend of Satellite-Derived
- 726 Chlorophyll-a and Hypoxia Off the Changjiang Estuary, ESTUARIES AND COASTS,
- 727 40, 1055-1065, 10.1007/s12237-016-0203-0, 2017.
- 728 Chen, L., Zhang, X., He, B., Liu, J., Lu, Y., Liu, H., Dai, M., Gan, J., and Kao, S.-J.:
- 729 Dark Ammonium Transformations in the Pearl River Estuary During Summer, Journal
- 730 of Geophysical Research: Biogeosciences, 125, e2019JG005596,
- 731 https://doi.org/10.1029/2019JG005596, 2020.
- 732 Chen, Z., Yu, L., and Hu, J.: Disentangling the contributions of anthropogenic nutrient
- 733 input and physical forcing to long-term deoxygenation off the Pearl River Estuary,
- 734 China, Water Research, 265, 122258, https://doi.org/10.1016/j.watres.2024.122258,
- 735 2024.

- 736 Cheung, Y. Y., Cheung, S., Mak, J., Liu, K., Xia, X., Zhang, X., Yung, Y., and Liu, H.:
- 737 Distinct interaction effects of warming and anthropogenic input on diatoms and
- dinoflagellates in an urbanized estuarine ecosystem, Global Change Biology, 27, 3463-
- 739 3473, 10.1111/gcb.15667, 2021.
- 740 Cormier, J. M., Coffin, M. R. S., Pater, C. C., Knysh, K. M., Gilmour, R. F., Guyondet,
- 741 T., Courtenay, S. C., and van den Heuvel, M. R.: Internal nutrients dominate load and
- drive hypoxia in a eutrophic estuary, Environmental Monitoring and Assessment, 195,
- 743 1211, 10.1007/s10661-023-11621-y, 2023.
- 744 Cullen, J. J.: Subsurface Chlorophyll Maximum Layers: Enduring Enigma or Mystery
- 745 Solved?, in: ANNUAL REVIEW OF MARINE SCIENCE, VOL 7, edited by: Carlson,
- 746 C. A., and Giovannoni, S. J., 207-239, 10.1146/annurev-marine-010213-135111, 2015.
- 747 Dethier, E. N., Renshaw, C. E., and Magilligan, F. J.: Rapid changes to global river
- 748 suspended sediment flux by humans, Science, 376, 1447-1452,
- 749 10.1126/science.abn7980, 2022.
- 750 Diaz, R. J. and Rosenberg, R.: Spreading dead zones and consequences for marine
- 751 ecosystems, Science, 321, 926-929, 10.1126/science.1156401, 2008.
- 752 DiToro, D. M.: Sediment flux modeling, John Wiley & Sons2001.
- 753 Domingues, R. B., Barbosa, A. B., Sommer, U., and Galvão, H. M.: Phytoplankton
- 754 composition, growth and production in the Guadiana estuary (SW Iberia): Unraveling
- 755 changes induced after dam construction, Science of The Total Environment, 416, 300-
- 756 313, https://doi.org/10.1016/j.scitotenv.2011.11.043, 2012.
- 757 Fizpartick, J.: A user's guide for RCA (release 3.0), HydroQual Inc., New Jersey, USA.
- 758 217p, 2004.
- 759 Ge, J., Torres, R., Chen, C., Liu, J., Xu, Y., Bellerby, R., Shen, F., Bruggeman, J., and
- 760 Ding, P.: Influence of suspended sediment front on nutrients and phytoplankton
- 761 dynamics off the Changjiang Estuary: A FVCOM-ERSEM coupled model experiment,
- 762 Journal of Marine Systems, 204, 103292,
- 763 https://doi.org/10.1016/j.jmarsys.2019.103292, 2020.
- Hagy, J. D., Boynton, W. R., and Jasinski, D. A.: Modelling phytoplankton deposition
- 765 to Chesapeake Bay sediments during winter-spring: interannual variability in relation
- 766 to river flow, ESTUARINE COASTAL AND SHELF SCIENCE, 62, 25-40,
- 767 10.1016/j.ecss.2004.08.004, 2005.
- Hong, B., Liu, Z., Shen, J., Wu, H., Gong, W., Xu, H., and Wang, D.: Potential physical
- 769 impacts of sea-level rise on the Pearl River Estuary, China, Journal of Marine Systems,
- 770 201, 103245, 10.1016/j.jmarsys.2019.103245, 2020.
- Howarth, R., Chan, F., Conley, D. J., Garnier, J., Doney, S. C., Marino, R., and Billen,
- G.: Coupled biogeochemical cycles: eutrophication and hypoxia in temperate estuaries
- and coastal marine ecosystems, Frontiers in Ecology and the Environment, 9, 18-26,
- 774 https://doi.org/10.1890/100008, 2011.
- Hu, J. and Li, S.: Modeling the mass fluxes and transformations of nutrients in the Pearl
- 776 River Delta, China, Journal of Marine Systems, 78, 146-167,
- 777 https://doi.org/10.1016/j.jmarsys.2009.05.001, 2009.

- Hu, J., Li, S., and Geng, B.: Modeling the mass flux budgets of water and suspended
- sediments for the river network and estuary in the Pearl River Delta, China, Journal of
- 780 Marine Systems, 88, 252-266, https://doi.org/10.1016/j.jmarsys.2011.05.002, 2011.
- Hu, J., Zhang, Z., Wang, B., and Huang, J.: Long-term spatiotemporal variations in and
- expansion of low-oxygen conditions in the Pearl River estuary: a study synthesizing
- 783 observations during 1976–2017, Biogeosciences, 18, 5247-5264, 10.5194/bg-18-5247-
- 784 2021, 2021.
- 785 Huang, Y.-G., Yang, H.-F., Jia, J.-J., Li, P., Zhang, W.-X., Wang, Y. P., Ding, Y.-F., Dai,
- 786 Z.-J., Shi, B.-W., and Yang, S.-L.: Declines in suspended sediment concentration and
- 787 their geomorphological and biological impacts in the Yangtze River Estuary and
- 788 adjacent sea, Estuarine, Coastal and Shelf Science, 265, 107708,
- 789 https://doi.org/10.1016/j.ecss.2021.107708, 2022.
- 790 Kasai, M., Brierley, G. J., Page, M. J., Marutani, T., and Trustrum, N. A.: Impacts of
- 791 land use change on patterns of sediment flux in Weraamaia catchment, New Zealand,
- 792 CATENA, 64, 27-60, https://doi.org/10.1016/j.catena.2005.06.014, 2005.
- Lai, Y., Jia, Z., Xie, Z., Li, S., and Hu, J.: Water quality changes and shift in mechanisms
- 794 controlling hypoxia in response to pollutant load reductions: A case study for Shiziyang
- 795 Bay, Southern China, Science of The Total Environment, 842, 156774,
- 796 https://doi.org/10.1016/j.scitotenv.2022.156774, 2022.
- 797 Laurent, A., Fennel, K., Ko, D. S., and Lehrter, J.: Climate change projected to
- 798 exacerbate impacts of coastal eutrophication in the northern Gulf of Mexico, Journal of
- 799 Geophysical Research: Oceans, 123, 3408-3426, 2018.
- 800 Li, D., Gan, J., Hui, C., Yu, L., Liu, Z., Lu, Z., Kao, S.-j., and Dai, M.: Spatiotemporal
- 801 Development and Dissipation of Hypoxia Induced by Variable Wind-Driven Shelf
- 802 Circulation off the Pearl River Estuary: Observational and Modeling Studies, Journal
- 803 of Geophysical Research: Oceans, 126, e2020JC016700,
- 804 https://doi.org/10.1029/2020JC016700, 2021.
- 805 Li, G., Liu, J., Diao, Z., Jiang, X., Li, J., Ke, Z., Shen, P., Ren, L., Huang, L., and Tan,
- 806 Y.: Subsurface low dissolved oxygen occurred at fresh- and saline-water intersection of
- the Pearl River estuary during the summer period, Marine Pollution Bulletin, 126, 585-
- 808 591, 10.1016/j.marpolbul.2017.09.061, 2018.
- 809 Li, X., Lu, C., Zhang, Y., Zhao, H., Wang, J., Liu, H., and Yin, K.: Low dissolved
- 810 oxygen in the Pearl River estuary in summer: Long-term spatio-temporal patterns,
- 811 trends, and regulating factors, Marine Pollution Bulletin, 151, 110814,
- 812 https://doi.org/10.1016/j.marpolbul.2019.110814, 2020.
- 813 Liu, Z., Fagherazzi, S., Liu, X., Shao, D., Miao, C., Cai, Y., Hou, C., Liu, Y., Li, X., and
- 814 Cui, B.: Long-term variations in water discharge and sediment load of the Pearl River
- 815 Estuary: Implications for sustainable development of the Greater Bay Area, Frontiers
- 816 in Marine Science, 9, 983517, 10.3389/fmars.2022.983517, 2022.
- 817 Lu, Z., Gan, J., Dai, M., Liu, H., and Zhao, X.: Joint Effects of Extrinsic Biophysical
- 818 Fluxes and Intrinsic Hydrodynamics on the Formation of Hypoxia West off the Pearl
- 819 River Estuary, Journal of Geophysical Research: Oceans, 123, 6241-6259,

- 820 10.1029/2018jc014199, 2018.
- 821 Luo, X., Yang, Q., and Jia, L.: The Riverbed Evolution of the River-Network System
- in the Pearl River Delta, Sun Yat-sen Univeristy Press, Guangzhou, China, 2002.
- 823 Ma, C., Zhao, J., Ai, B., Sun, S., and Yang, Z.: Machine Learning Based Long-Term
- Water Quality in the Turbid Pearl River Estuary, China, Journal of Geophysical
- 825 Research: Oceans, 127, e2021JC018017, https://doi.org/10.1029/2021JC018017, 2022.
- Ma, R., Chen, Z., Wang, B., Xu, C., Jia, Z., Li, L., and Hu, J.: Spatiotemporal variations
- and controlling mechanism of low dissolved oxygen in a highly urbanized complex
- 828 river system, Journal of Hydrology: Regional Studies, 52, 101691,
- 829 https://doi.org/10.1016/j.ejrh.2024.101691, 2024.
- Murphy, R. R., Kemp, W. M., and Ball, W. P.: Long-Term Trends in Chesapeake Bay
- 831 Seasonal Hypoxia, Stratification, and Nutrient Loading, ESTUARIES AND COASTS,
- 832 34, 1293-1309, 10.1007/s12237-011-9413-7, 2011.
- Pitcher, G. C., Aguirre-Velarde, A., Breitburg, D., Cardich, J., Carstensen, J., Conley,
- 834 D. J., Dewitte, B., Engel, A., Espinoza-Morriberón, D., Flores, G., Garçon, V., Graco,
- 835 M., Grégoire, M., Gutiérrez, D., Hernandez-Ayon, J. M., Huang, H.-H. M., Isensee, K.,
- Jacinto, M. E., Levin, L., Lorenzo, A., Machu, E., Merma, L., Montes, I., Swa, N.,
- 837 Paulmier, A., Roman, M., Rose, K., Hood, R., Rabalais, N. N., Salvanes, A. G. V.,
- 838 Salvatteci, R., Sánchez, S., Sifeddine, A., Tall, A. W., Plas, A. K. v. d., Yasuhara, M.,
- 839 Zhang, J., and Zhu, Z. Y.: System controls of coastal and open ocean oxygen depletion,
- Progress in Oceanography, 197, 102613, https://doi.org/10.1016/j.pocean.2021.102613,
- 841 2021.
- Roman, M. R., Brandt, S. B., Houde, E. D., and Pierson, J. J.: Interactive effects of
- 843 Hypoxia and temperature on coastal pelagic zooplankton and fish, Frontiers in Marine
- 844 Science, 6, 10.3389/fmars.2019.00139, 2019.
- 845 Su, J., Dai, M., He, B., Wang, L., Gan, J., Guo, X., Zhao, H., and Yu, F.: Tracing the
- origin of the oxygen-consuming organic matter in the hypoxic zone in a large eutrophic
- estuary: the lower reach of the Pearl River Estuary, China, Biogeosciences, 14, 4085-
- 848 4099, 10.5194/bg-14-4085-2017, 2017.
- 849 Syvitski, J. P. M. and Kettner, A.: Sediment flux and the Anthropocene, Philosophical
- 850 Transactions of the Royal Society A: Mathematical, Physical and Engineering Sciences,
- 851 369, 957-975, doi:10.1098/rsta.2010.0329, 2011.
- Wang, B., Hu, J., Li, S., and Liu, D.: A numerical analysis of biogeochemical controls
- with physical modulation on hypoxia during summer in the Pearl River estuary,
- 854 Biogeosciences, 14, 2979-2999, 10.5194/bg-14-2979-2017, 2017.
- Wang, B., Hu, J., Li, S., Yu, L., and Huang, J.: Impacts of anthropogenic inputs on
- hypoxia and oxygen dynamics in the Pearl River estuary, Biogeosciences, 15, 6105-
- 857 6125, 10.5194/bg-15-6105-2018, 2018.
- Wang, G., Cao, W., Yang, Y., Zhou, W., Liu, S., and Yang, D.: Variations in light
- absorption properties during a phytoplankton bloom in the Pearl River estuary,
- 860 Continental Shelf Research, 30, 1085-1094, 2010.
- 861 Wang, H., Dai, M., Liu, J., Kao, S.-J., Zhang, C., Cai, W.-J., Wang, G., Qian, W., Zhao,

- 862 M., and Sun, Z.: Eutrophication-Driven Hypoxia in the East China Sea off the
- 863 Changjiang Estuary, Environmental Science & Technology, 50, 2255-2263,
- 864 10.1021/acs.est.5b06211, 2016.
- Wang, J. J., Bouwman, A. F., Liu, X. C., Beusen, A. H. W., Van Dingenen, R., Dentener,
- 866 F., Yao, Y. L., Glibert, P. M., Ran, X. B., Yao, Q. Z., Xu, B. C., Yu, R. C., Middelburg,
- J. J., and Yu, Z. G.: Harmful Algal Blooms in Chinese Coastal Waters Will Persist Due
- 868 to Perturbed Nutrient Ratios, ENVIRONMENTAL SCIENCE & TECHNOLOGY
- 869 LETTERS, 8, 276-284, 10.1021/acs.estlett.1c00012, 2021.
- 870 Wang, K., Chen, J., Jin, H., Li, H., Gao, S., Xu, J., Lu, Y., Huang, D., Hao, Q., and
- Weng, H.: Summer nutrient dynamics and biological carbon uptake rate in the
- 872 Changjiang River plume inferred using a three end-member mixing model, Continental
- 873 Shelf Research, 91, 192-200, https://doi.org/10.1016/j.csr.2014.09.013, 2014.
- Wang, Y., Wu, H., Lin, J., Zhu, J., Zhang, W., and Li, C.: Phytoplankton Blooms off a
- 875 High Turbidity Estuary: A Case Study in the Changjiang River Estuary, Journal of
- 876 Geophysical Research: Oceans, 124, 8036-8059, 10.1029/2019jc015343, 2019.
- 877 Wen, G., Liang, Z., Xu, X., Cao, R., Wan, Q., Ji, G., Lin, W., Wang, J., Yang, J., and
- Huang, T.: Inactivation of fungal spores in water using ozone: Kinetics, influencing
- 879 factors and mechanisms, Water Research, 185, 116218,
- 880 https://doi.org/10.1016/j.watres.2020.116218, 2020.
- Wu, C. S., Yang, S., Huang, S., and Mu, J.: Delta changes in the Pearl River estuary and
- its response to human activities (1954–2008), Quaternary International, 392, 147-154,
- 883 https://doi.org/10.1016/j.quaint.2015.04.009, 2016.
- Yang, H., Wang, T., Yang, D., Yan, Z., Wu, J., and Lei, H.: Runoff and sediment effect
- of the soil-water conservation measures in a typical river basin of the Loess Plateau,
- 886 CATENA, 243, 108218, https://doi.org/10.1016/j.catena.2024.108218, 2024.
- 887 Yu, L., Gan, J., 2022. Reversing impact of phytoplankton phosphorus limitation on
- coastal hypoxia due to interacting changes in surface production and shoreward bottom
- 889 oxygen influx. Water Res. 118094 https://doi.org/10.1016/j. watres.2022.118094.
- 890 Yu, L., Fennel, K., Laurent, A., 2015. A modeling study of physical controls on hypoxia
- generation in the northern Gulf of Mexico. J. Geophys. Res. Oceans 120, 5019–5039.
- 892 https://doi.org/10.1002/2014JC010634.
- 893 Yu, L., Gan, J., Dai, M., Hui, C., Lu, Z., Li, D., 2020. Modeling the role of riverine
- 894 organic matter in hypoxia formation within the coastal transition zone off the Pearl
- 895 River Estuary. Limnol. Oceanogr. 9999, 1–17. https://doi.org/10.1002/lno.11616
- 896 Zhang, S., Lu, X. X., Higgitt, D. L., Chen, C.-T. A., Han, J., and Sun, H.: Recent
- 897 changes of water discharge and sediment load in the Zhujiang (Pearl River) Basin,
- 898 China, Global and Planetary Change, 60, 365-380,
- 899 https://doi.org/10.1016/j.gloplacha.2007.04.003, 2008.
- 200 Zhang, Z., Wang, B., Li, S., Huang, J., and Hu, J.: On the Intra-annual Variation of
- 901 Dissolved Oxygen Dynamics and Hypoxia Development in the Pearl River Estuary,
- 902 Estuaries and Coasts, 45, 1305-1323, 10.1007/s12237-021-01022-0, 2022.